RECENT RESULTS FROM THE NOMAD EXPERIMENT

Burkhard Schmidt
Institute for Physics, Dortmund University
D–44221 Dortmund, Germany

Representing the NOMAD Collaboration

ABSTRACT

NOMAD is a short baseline neutrino oscillation experiment searching for $\nu_\mu \to \nu_\tau$ and $\nu_\mu \to \nu_e$ oscillations in the CERN SPS wide band neutrino beam. The experiment has been collecting data since July 1995 and the data taking will continue until at least the end of 1997.

A preliminary analysis based on the 1995 data sample allows NOMAD to set 90% confidence limits of $\sin^2 2\theta_{\mu\tau} < 3.4\times10^{-3}$ for $\nu_\mu \to \nu_\tau$ and $\sin^2 2\theta_{\mu e} < 2\times10^{-3}$ for $\nu_\mu \to \nu_e$ oscillations at large Δm^2.

1 Introduction

The Neutrino Oscillation MAgnetic Detector (NOMAD, WA-96)[1] was designed to search for ν_τ appearing from $\nu_\mu \rightarrow \nu_\tau$ oscillations in the CERN SPS wide band neutrino beam, which consists primarily of ν_μ neutrinos with a small ν_e component (less than $\sim 1\%$) and a negligible ($\sim 5 \times 10^{-6}$) contamination of prompt[2] ν_τ. If $\nu_\mu \rightarrow \nu_\tau$ oscillations occur, ν_τ's would be detected via their charged current (CC) interactions $\nu_\tau + N \rightarrow \tau^- + X$ in an active target using the kinematical characteristics of the subsequent τ^- decays.

Under the assumption of two-flavor mixing, the probability of oscillation as a function of the distance L from the neutrino production point to its interaction point is given by:

$$P = \sin^2(2\theta) \cdot \sin^2(\pi L/\lambda); \quad \lambda[\mathrm{km}] = 2.48 \cdot E[\mathrm{GeV}]/\Delta m^2[\mathrm{eV}^2],$$

where θ is the mixing angle, λ is the oscillation length, E is the neutrino energy, and Δm^2 is the neutrino mass squared difference. Located at a distance of 640 m from the average neutrino production point and using a mean ν_μ energy of 24 GeV (Fig. 1), NOMAD is sensitive to the cosmologically interesting ν_τ mass range $\Delta m^2 \sim 10 \div 100$ eV^2. If no evidence for $\nu_\mu \rightarrow \nu_\tau$ oscillations is found, NOMAD is expected to reach a sensitivity to oscillation parameters of $\sin^2 2\theta_{\mu\tau} < 3.8 \times 10^{-4}$ for $\Delta m^2 \geq 40$ eV^2 (Fig. 2).

In order to exploit the low ν_e contamination in the CERN-SPS wide band neutrino beam, the detector has been optimized to efficiently detect electrons and, in particular, ν_e charged current interactions. Their analysis is relevant for the search for $\nu_\mu \rightarrow \nu_e$ oscillations, since an oscillation signal would manifest itself both as an excess of events in the ν_e CC sample and as a change in the shape of the ν_e CC energy spectrum. The interest for this kind of study has increased markedly, following the LSND[4] Collaboration claim for evidence for $\bar{\nu}_\mu \rightarrow \bar{\nu}_e$ oscillations. NOMAD is sensitive to a large fraction of the parameter region corresponding to the LSND most probable values in the $(\sin^2 2\theta, \Delta m^2)$ plane. In case of $\nu_\mu \rightarrow \nu_e$ oscillations with $\Delta m^2 > 10$ eV^2 and with the probability of 3×10^{-3} observed by LSND, a signal should be seen in the NOMAD data.

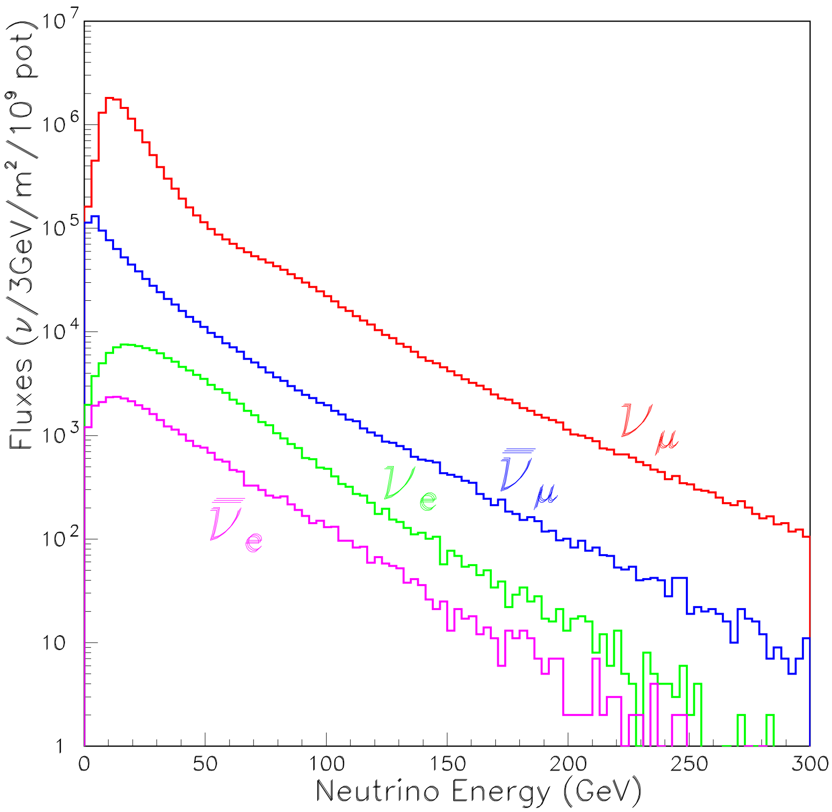

Figure 1: Monte Carlo predictions of the CERN-SPS wide band neutrino beam. Fluxes are given for 10^9 protons on target (p.o.t.) and are averaged over the NOMAD area ($2.6 \times 2.6\ m^2$).

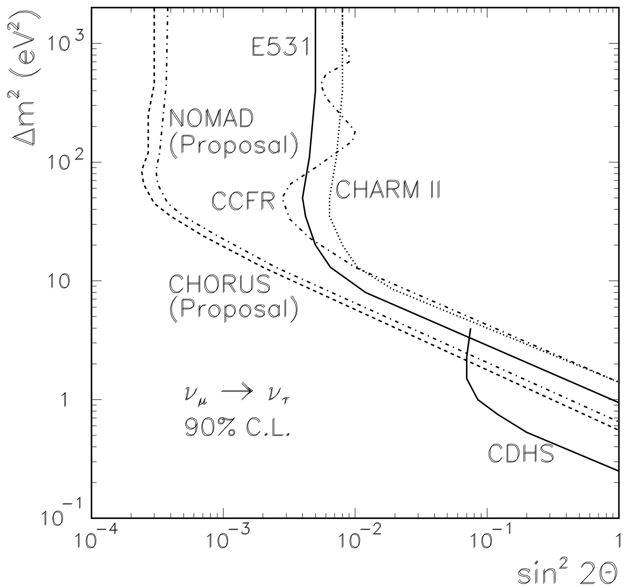

Figure 2: Current 90% C.L. neutrino oscillation parameter limits[3] compared to the limits achievable by the CHORUS and NOMAD experiments.

2 The Detector

The NOMAD detector is described in detail elsewhere.[5] It consists of a number of subdetectors, most of which are located in a dipole magnet with a field volume of $7.5 \times 3.5 \times 3.5$ m^3 (see Fig. 3).

The target part of the detector was designed to accommodate two requirements: to be as light as possible (low density and low atomic number materials) in order to give precise measurements of the momenta of charged tracks and to avoid photon conversions and secondary interactions, and to be as heavy as possible to produce a significant number of neutrino interactions. The compromise was achieved using an active target (2.7 tons) of 3×3 m^2 wire drift chambers (DC), with the target mass given by the chamber structure, a sandwich of honeycomb panels, and kevlar-epoxy resin skins. Placed inside the magnetic field of 0.4 T, these chambers provide good position resolution (< 200 μm along the drift direction for incident angles less than 10°) and momentum resolution ($\sim 3.5\%$ in

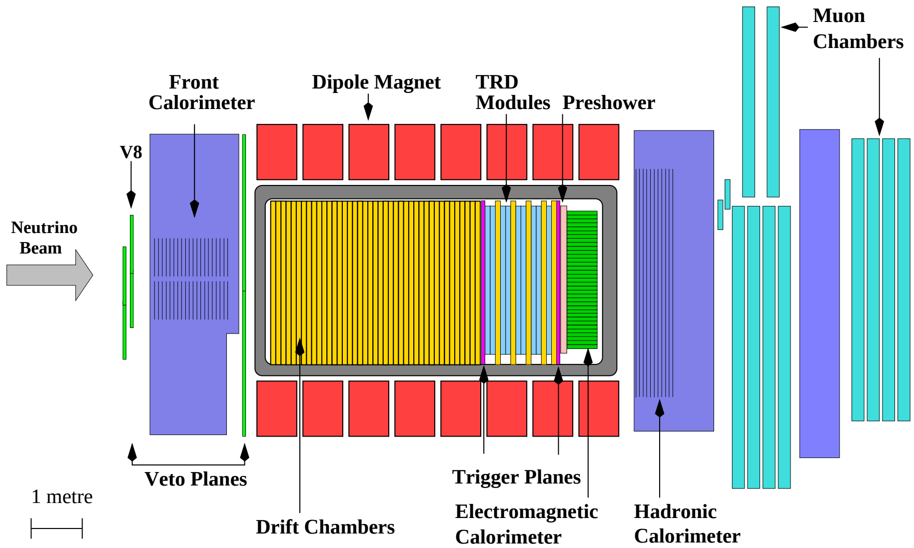

Figure 3: Side view of the NOMAD detector.

the momentum range $p < 10$ GeV/c), as measured from the 1995 data sample, Fig. 4.

The searches for $\nu_\mu \to \nu_\tau$ and $\nu_\mu \to \nu_e$ oscillations in NOMAD rely strongly on electron and muon identification, as well as on an accurate measurement of the energy flow in an event. The basic electron identification is performed using the transition radiation detector (TRD). The preshower (PRS) and the lead-glass electromagnetic calorimeter (ECAL) are used to improve the electron identification and to provide the measurement of electron energy together with the reconstruction of electromagnetic showers induced by photons.

The TRD consists of nine identical modules, each module comprising a radiator followed by a detection plane made of 176 straw tubes filled with an 80% xenon – 20% methane gas mixture. The electron identification by the TRD is based on the difference of energy deposited in the straw tubes by particles of different Lorentz factors $\gamma = E/m$ (Fig. 5). The NOMAD TRD provides a 10^3 pion rejection factor for a 90% electron efficiency, for isolated tracks in the momentum range $1 \div 50$ GeV/c.

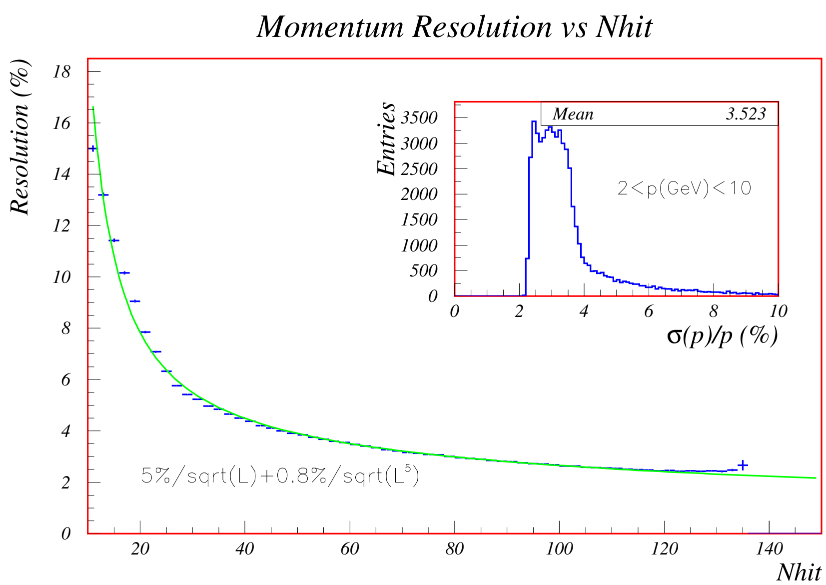

Figure 4: Momentum resolution as a function of the track length (number of hits in the fiducial volume of drift chambers).

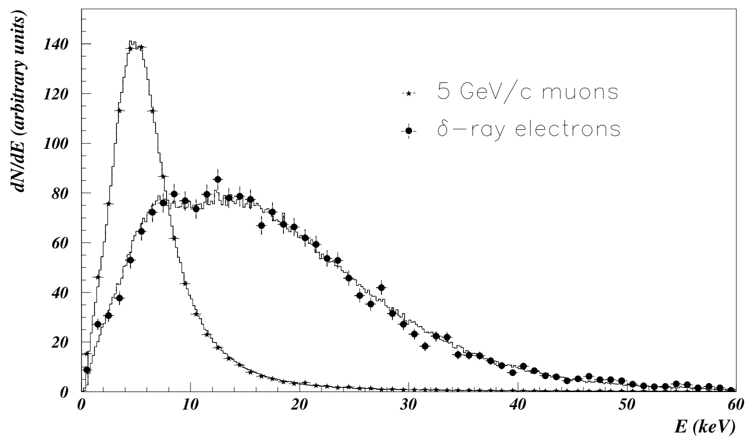

Figure 5: Energy deposition in a TRD detection plane for 5 GeV/c muons and 2 GeV/c δ-ray electrons from data compared to a Monte Carlo simulation.

The preshower is composed of two planes of proportional tubes preceded by a 9 mm (1.6 X_0) lead-antimony (96%–4%) converter. The electromagnetic calorimeter consists of 875 lead-glass Cherenkov counters with a rectangular cross-section of 79×112 mm^2 and 19 radiation lengths deep. The PRS and ECAL system provides an additional π/e separation factor of $10^2 \div 10^3$ and an energy resolution of $\sigma(E)/E = 3.2\%/\sqrt{E(\mathrm{GeV})} \oplus 1\%$.

The iron wall downstream of the magnet has been instrumented to provide a hadron calorimeter (HCAL) intended to measure neutral hadrons which could generate fake missing momentum in the transverse plane p_T^{miss}. The muon detector is a set of 10 drift chambers arranged in two stations separated by a 80-cm-thick iron wall. It provides segments and hits which can be associated to extrapolated DC tracks and are used to identify muons or to veto candidate hadrons. Finally, the pillar in front of the magnet has also been instrumented (front calorimeter) to allow a study of multi-muon physics and a search for neutral heavy objects produced in neutrino interactions.

The veto (V) and the two trigger planes (T_1 and T_2) are used to select neutrino interactions inside the fiducial volume of the detector with the requirement $\overline{V} \times T_1 \times T_2$.

3 Detector Performance

During the 1995 run, the NOMAD experiment collected data for a total exposure of 0.86×10^{19} protons on target (p.o.t.), out of which a clean sample of about 1.6×10^5 neutrino interactions in the fiducial volume was selected.

Charged current ν_μ and $\bar{\nu}_\mu$ candidates were selected by requiring one matched track between the drift chambers and the muon chambers with a momentum larger than 2.5 GeV/c. An example of a reconstructed ν_μ CC candidate event is shown in Fig. 6. The experimental distribution of the muon momentum given in Fig. 7 agrees well with the Monte Carlo (MC) predictions.

Specific studies of the vertex resolution (Fig. 8) and of the K_s^0's, Λ's, and π^0's (Figs. 9 and 10) were made to control the overall quality of the reconstruction and of the detector performance. Mass resolutions in agreement with the measured (and expected) momentum/energy resolution were obtained.

About 4.7×10^5 neutrino interactions were recorded in 1996 and are being analyzed.

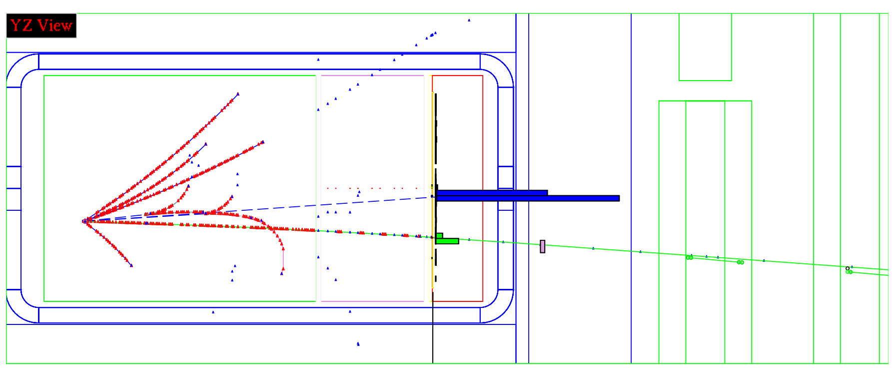

Figure 6: A reconstructed ν_μ CC candidate. The longest track at the bottom is a muon matched to the segments in the muon chambers; the small triangles are track extrapolations. Two photons (dashed lines) were built: one out of the stand-alone ECAL cluster, the other from the conversion inside the DC fiducial volume.

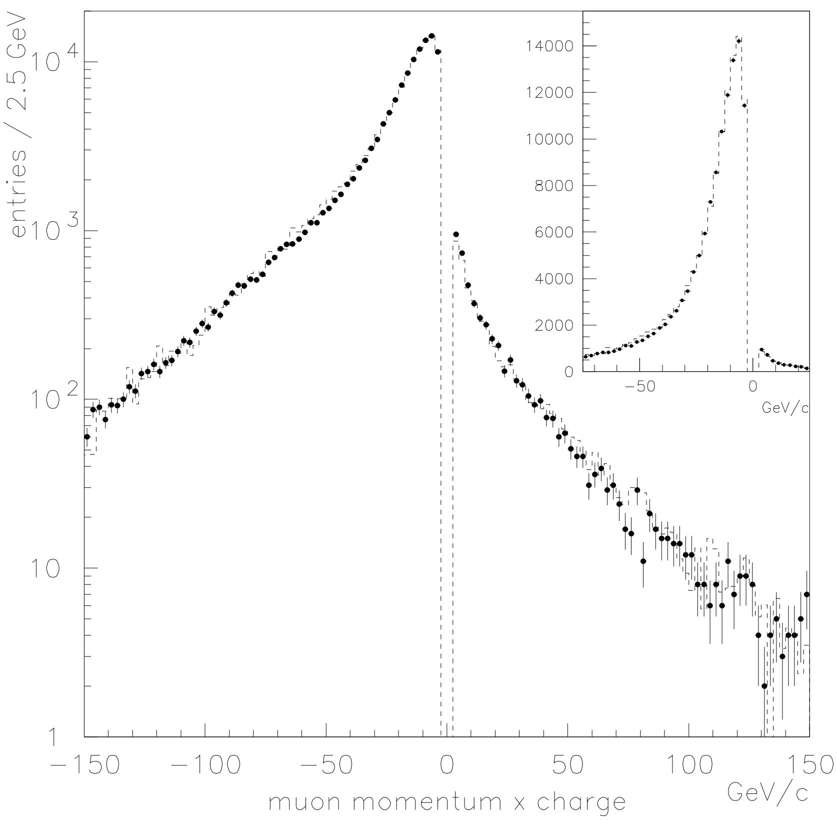

Figure 7: Inclusive muon momentum spectrum signed by the charge of the track.

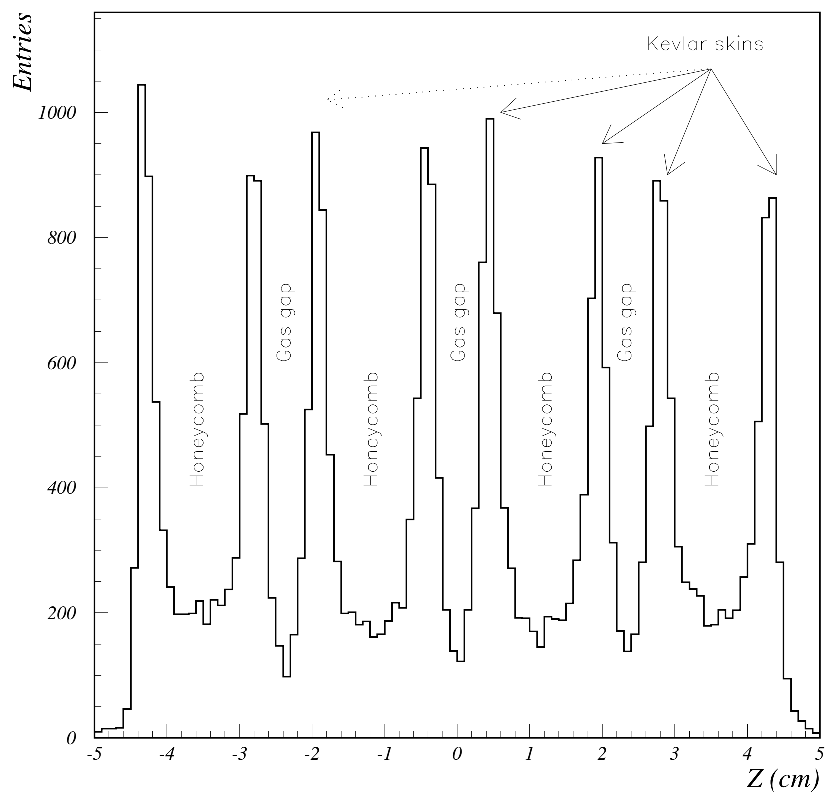

Figure 8: Longitudinal primary vertex distribution folded modulo one chamber. The chamber structure is clearly visible.

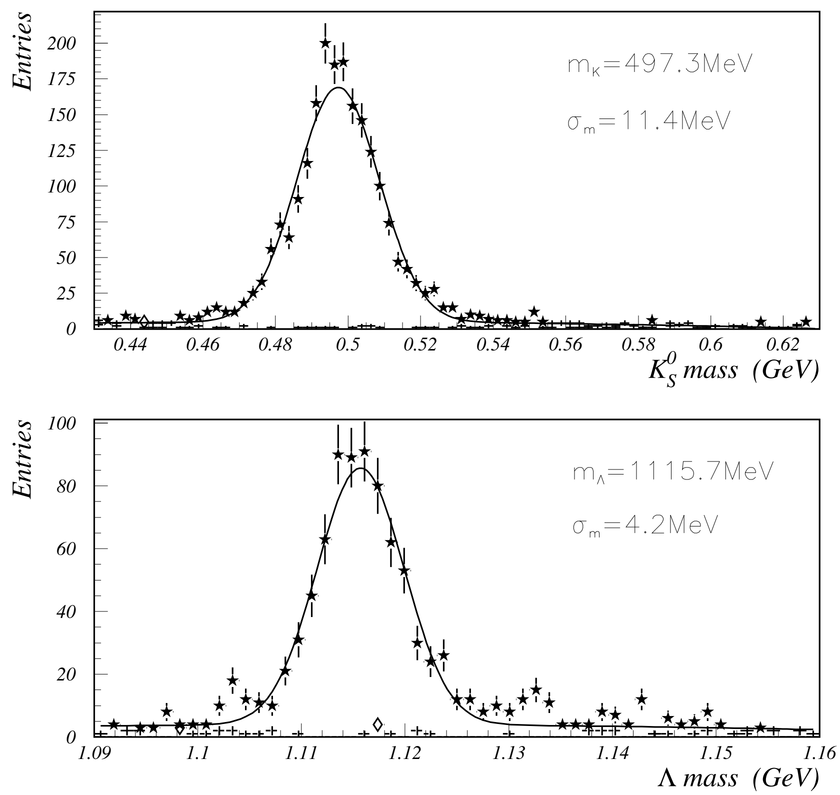

Figure 9: Reconstruction of $V^0(+-)$ secondary vertices under the $\pi^+\pi^-$ (top) and $p\pi^-$ (bottom) assumptions showing clear K^0_s and Λ peaks. Background from the same sign ($++$ and $--$) combinations is also shown.

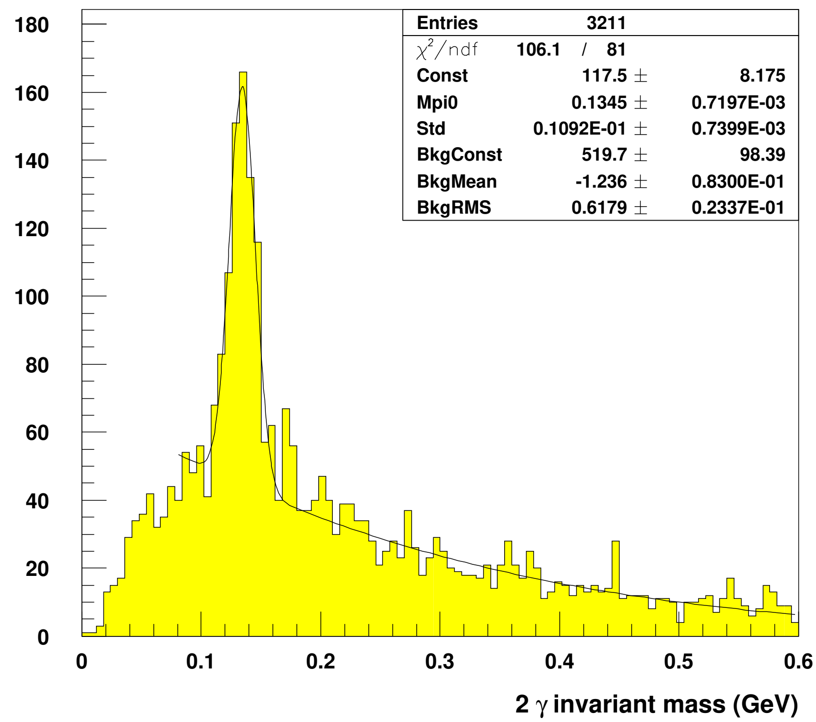

Figure 10: Invariant mass distribution of two photons reconstructed in the electromagnetic calorimeter showing a clear π^0 peak.

4 Search for $\nu_\mu \to \nu_e$ Oscillations

Since the search for $\nu_\mu \to \nu_e$ oscillations implies a direct comparison between the observed and the expected spectra, knowledge of the beam characteristics is crucial.

The neutrinos are primarily produced from the decays in flight of the secondary π and K mesons originating from 450 GeV protons impinging on a beryllium target. The positive component of the secondary beam is focused by a system of magnetic lenses (the *horn* and the *reflector*). Most of the mesons will decay then in a 290 m long vacuum tunnel. The residual charged particles are finally stopped by a thick shield, placed before the experimental site, where only neutrinos can penetrate.

A Monte Carlo package has been developed to describe the entire beam line: it is based on the GEANT[7] library for the detectors and the material description, and makes use of the FLUKA[8] package to simulate hadronic interactions. As already mentioned, the ν_e/ν_μ contamination is of the order of 1%; furthermore, the ν_e spectrum is harder than the ν_μ's ($< E_{\nu_e} > \quad \approx 37$ GeV), increasing the sensitivity of the experiment in the energy range relevant for the oscillation search. Since electron neutrinos mainly come from K decays, the fraction of ν_e's in the beam is determined by the kaon content of the secondary meson flux. At the present time, the K/π ratio in the relevant kinematic region is known with a systematic uncertainty of 10%; further constraints are expected soon from the NA56[9] Collaboration, which has studied p-Be interactions for 450 GeV/c protons and secondary particles with momenta below 40 GeV/c.

Another possible approach tries to use data itself to extract beam information and predict the ν_e spectrum in the absence of oscillations. The way this can be done is illustrated in Fig. 11, where neutrino- and antineutrino spectra are given in terms of parent particles: since possible oscillations are suppressed in the antineutrino sample, because of the large $\bar{\nu}_e/\bar{\nu}_\mu$ ratio, one can deduce all the relevant information using only events with a primary μ^-, μ^+ or e^+ (**not** e^-). In fact, the K^+ content can be constrained by the high energy ν_μ spectrum, while the low energy part fixes the π^+ (and hence the μ^+) content of the beam. In a similar way, combined information from $\bar{\nu}_\mu$ and $\bar{\nu}_e$ spectra allows one to extract the K^0_L component. Once the contributions from all parents are known, the expected ν_e energy distribution in absence of oscillations can be computed.

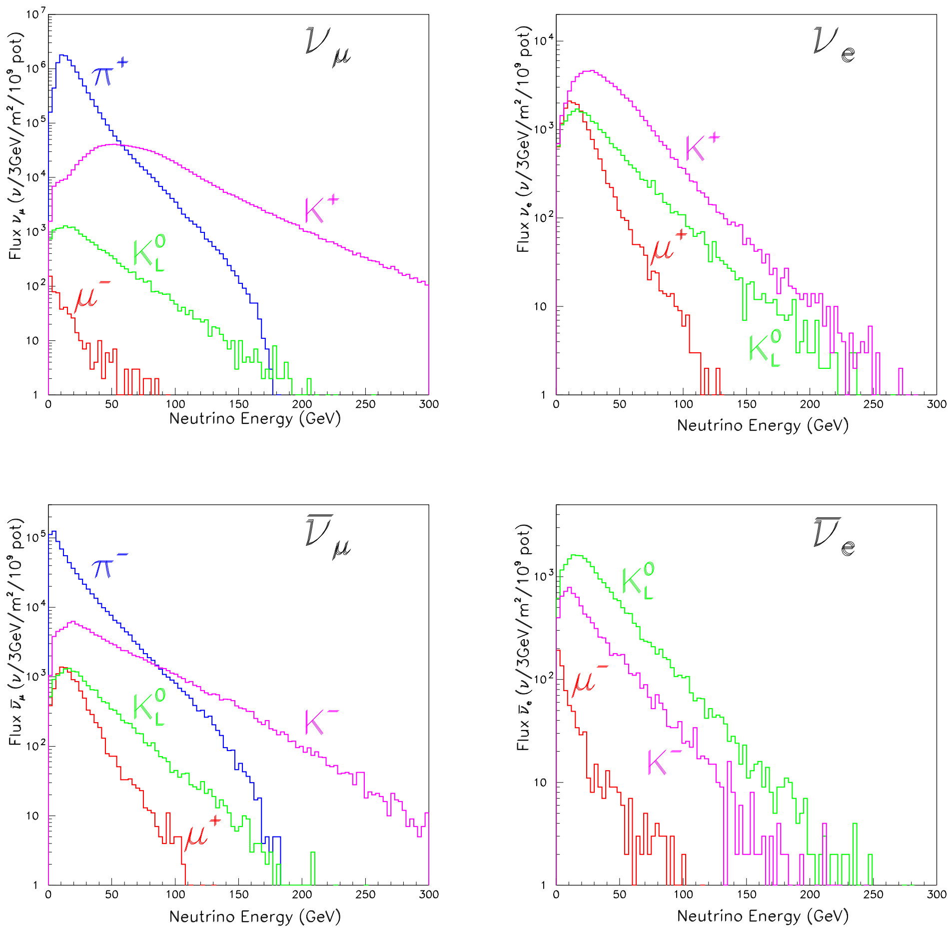

Figure 11: Contribution of parent particles to the different beam components.

If oscillations occur with parameters in the large Δm^2 range of LSND solutions, a significant effect should be observed in the measured ν_e CC total energy spectrum. For example, in case of oscillations with $\sin^2 2\theta = 0.006$ and $\Delta m^2 = 19$ eV^2, the number of ν_e charged current interactions would approximately double for $10 < E_\nu < 40$ GeV.

In order to reduce systematic uncertainties, it is preferable to study the ratio between the number of ν_e and ν_μ charged current interactions as a function of the neutrino energy:

$$\mathcal{R}_{e\mu}(E_\nu) = \left[\frac{\# \quad \nu_e \text{ CC events}}{\# \quad \nu_\mu \text{ CC events}}\right](E_\nu). \tag{1}$$

In our analysis, the neutrino energy E_ν is approximated on an event-by-event basis by the visible energy in the event, namely the sum of the energies of the charged lepton and of the observed hadrons in the final state. In Fig. 12, the ratio measured with the data sample collected during the 1995 data taking (grey circles) is superimposed on the one expected in the absence of oscillations, for which the size of systematic uncertainties is also given (area between solid histograms); error bars on data points include statistical errors only. For comparison, the expected $\mathcal{R}_{e\mu}$ for oscillations with $\sin^2 2\theta = 0.006$ and $\Delta m^2 = 19$ eV^2 is also given (black squares). The measured ratio fits expectations well, meaning that no evidence for oscillations is observed in NOMAD data.

A statistical comparison of the measured $\mathcal{R}_{e\mu}$ to what is expected for different values of the oscillation parameters allows one to compute an exclusion plot on the $(\sin^2 2\theta, \Delta m^2)$ plane. A preliminary curve is shown in Fig. 13; the only systematic error taken into account is a 10% error on the K/π ratio. The limit set corresponds to $\sin^2 2\theta < 2 \times 10^{-3}$ for large values of Δm^2. For comparison, the limits obtained by other experiments[10] and the LSND-allowed solutions are drawn as well.

5 Search for $\nu_\mu \to \nu_\tau$ Oscillations

The selection of ν_τ CC interactions in NOMAD relies only on kinematic criteria. A careful study of event kinematics, particle isolation, and momentum balance in the transverse plane allows one to distinguish the ν_τ CC interactions from ν_μ and ν_e CC or neutral current (NC) background events.

Using accurate measurements of charged particle momenta and total energy flow, as well as the possibility to identify electrons and muons with high efficiency and high purity, NOMAD is able to search for τ^- decays into two leptonic channels: $e^-\nu_\tau\bar{\nu}_e$ and $\mu^-\nu_\tau\bar{\nu}_\mu$, and into three hadronic ones: $\pi^-\nu_\tau$, $\rho^-\nu_\tau$, and $\pi^-\pi^-\pi^+(n\pi^0)\nu_\tau$, i.e., about 88% of the τ decays.

A preliminary $\nu_\mu \to \nu_\tau$ oscillation search was performed on the 1995 data sample.

5.1 Leptonic τ-Decay Modes

The $\tau^- \to e^-\nu_\tau\bar{\nu}_e$ analysis requires an identified electron in the detector, associated to the primary vertex. Photon conversions and Dalitz decays of π^0 are removed by demanding that the invariant mass of the electron and any other positively charged candidate track be greater than 0.1 GeV/c^2. Asymmetric pairs with an unreconstructed positron are rejected by the requirement that the p_T of the electron with respect to the momentum of the hadron jet, q_T, be greater than 0.75 GeV. Background from ν_e CC is reduced by demanding $E_{vis} < 40$ GeV. The transverse mass, m_T, formed from $\vec{p_T^e}$ and $\vec{p_T^{miss}}$, must be smaller than 1.7 GeV. Finally, a cut in the ϕ_{eh}–ϕ_{mh} plane is applied to remove the remaining ν_e CC background events, as shown in Fig. 14. We define ϕ_{eh} as the angle between the electron and the hadron resultant transverse momenta, and ϕ_{mh} as the angle between the missing transverse momentum and the hadron transverse momentum. No candidates are found in the data (0.4 background events expected).

For the $\tau^- \to \mu^-\nu_\tau\bar{\nu}_\mu$ analysis, an identified muon with momentum greater than 3 GeV/c is required; the kinematical cuts are similar to the ones used in the electron channel, but are harder in order to compensate for higher background. In particular, an explicit cut on $\vec{p_T^{miss}} > 1.7$ GeV is used. Again, no candidates are observed.

5.2 Hadronic τ-Decay Modes

In the $\tau^- \to \pi^-\nu_\tau$ analysis, the leading negatively charged particle with $p >$ 3 GeV/c that is not a muon or electron is taken as a π^- candidate. The $(\pi^-\nu)$ system is required to be consistent with τ^- decay in the transverse plane: the transverse mass $M_T = \sqrt{(p_T^\pi + p_T^\nu)^2 - (\vec{p_T^\pi} + \vec{p_T^\nu})^2}$ should be less than 2.5 GeV, where $\vec{p_T^\nu}$ is the missing momentum in the transverse plane. To reject the background from ν_μ and $\bar{\nu}_\mu$ CC interactions with a lost $\mu^\pm$, all events where it is not possible to identify the highest p_T track as a muon (either because the momentum is too low or the track misses the muon chambers) are removed. The cut on the transverse momentum component Q_T of the π^- candidate with respect to the total momentum,

$$Q_T = \sqrt{(\vec{p^\pi})^2 - (\vec{p^\pi} \cdot \vec{p_{tot}})^2 / p_{tot}^2},$$

is imposed in order to reject background from NC interactions in which the π^- candidate is a part of the hadron jet. The Q_T distributions for the samples of simulated ν_μ NC events, simulated ν_μ CC events with muon removed ("fake NC") and "data simulator" (real ν_μ CC events with muon removed) are presented in Fig. 15. The agreement between these distributions demonstrates that the Monte Carlo simulation describes the data correctly in the Q_T variable. The Q_T distributions for simulated $\tau^- \to \pi^-\nu_\tau$ decays and NOMAD data are shown in Fig. 15. After the requirement $Q_T > 1.7$ GeV there are no expected background events left and no survivors in the data.

For the analysis of the $\tau^- \to \pi^-\pi^-\pi^+(n\pi^0)\nu_\tau$ channel, three pion candidates are selected based on the structure of the $\pi^-\pi^-\pi^+$ system, i.e., its invariant mass and opening angle, the angle of the candidate with respect to the hadron jet, and the fraction of the total momentum carried by the 3π system. The background from ν_μ NC interactions is rejected by imposing cuts on the 3π structure, momentum balance in the transverse plane, and by demanding the 3π system to be isolated from the hadron jet. The charged current ν_μ CC and ν_e CC interactions with a lost primary lepton are rejected by tight muon and electron vetos applied to the two highest p_T tracks in an event. No candidates are observed in the data with 0.5 background events expected.

5.3 Combined Sensitivity

A τ^- search was also performed in a sample of low multiplicity events (less than four primary tracks) enriched by quasi-elastic events and resonance production. The advantage of using this sample, compared to the high multiplicity sample dominated by deep inelastic scattering, is a simpler event topology, lower background, and larger $\sigma(\nu_\tau)/\sigma(\nu_\mu)$ ratio.

The oscillation probability in the case of no observed signal can be written as

$$P_{osc} < \frac{N_\tau}{(N_\mu/\varepsilon_\mu) \times (\sigma(\nu_\tau)/\sigma(\nu_\mu)) \times \Sigma_i(Br_i \times \epsilon_i)},$$

where N_τ is an upper limit on the possible number of τ decays, N_μ is the observed number of ν_μ CC interactions in the fiducial volume, ε_μ is the identification efficiency for ν_μ CC events, $\sigma(\nu_\tau)/\sigma(\nu_\mu)$ is the kinematic suppression factor due to the differences between the τ and μ masses, Br_i is the branching ratio, and ϵ_i is the selection efficiency for the i-th decay mode of the τ.

Decay mode	Br	$(N_\mu/\varepsilon_\mu)Br < \sigma(\nu_\tau)/\sigma(\nu_\mu)\epsilon >$
$\tau^- \to e^-\nu_\tau\bar{\nu}_e$	0.178	659
$\tau^- \to \mu^-\nu_\tau\bar{\nu}_\mu$	0.174	123
$\tau^- \to \pi^-(K^-)\nu_\tau$, $\tau^- \to \rho^-\nu_\tau^*$	0.378	410
$\tau^- \to \pi^-\pi^-\pi^+(n\pi^0)\nu_\tau$	0.149	249
TOTAL	0.879	1441

* Analysis optimized for $\tau^- \to \pi^-\nu_\tau$ decay.

Table 1: Sensitivity for τ^- decay channels.

No candidate events were observed in the 1995 data sample, while the estimated total background amounts to one event. In order to reliably determine the expected backgrounds and the resulting τ selection efficiencies, ν_μ CC data events are used as a simulator to cross-check Monte Carlo estimations. The sensitivity for different decay channels is given in Table 1. The uncertainty on the sensitivity is about 20%, resulting from the uncertainty of the efficiency calculations. Due to this fact, the upper limit on the number of possible τ^- candidates at 90% confidence level is increased[11] from 2.3 to 2.41. The preliminary limit on the probability of $\nu_\mu \to \nu_\tau$ oscillations is then:

$$P_{osc}(\nu_\mu \to \nu_\tau) = 2.41/1441 < 1.7 \times 10^{-3},$$

which corresponds to $\sin^2 2\theta_{\mu\tau} < 3.4 \times 10^{-3}$ for large Δm^2 at 90% C.L.

6 Conclusion

A preliminary analysis of the 1995 data results in an upper limit on $\sin^2 2\theta_{\mu\tau} < 3.4 \times 10^{-3}$ for $\nu_\mu \rightarrow \nu_\tau$ oscillations at large Δm^2 at 90% C.L. For $\nu_\mu \rightarrow \nu_e$ oscillations, a preliminary limit on the oscillation parameters has been calculated, giving $\sin^2 2\theta_{\mu e} < 2 \times 10^{-3}$ at large Δm^2 (90% C.L.) and excluding the reported LSND oscillation effect for $\Delta m^2 > 10$ eV^2.

The experimental data from the 1996 run are currently being analyzed. Data taking continued in 1997 and the NOMAD detector is performing well. With the 1996 and 1997 runs, the statistics will increase by a factor of five.

References

[1] NOMAD Coll., P. Astier *et al.*, *CERN-SPSLC/91-21* (1991);
Add. 1, *CERN-SPSLC/91-48* (1991);
Add. 2, *CERN-SPSLC/91-53* (1991).

[2] M. C. Gonzalez-Garcia and J. J. Gomez-Cadenas, Phys. Rev. D **55**, 1297 (1997);
B. Van de Vyver, Nucl. Instrum. Methods A **385**, 91 (1997).

[3] N. Ushida *et al.* (E531), Phys. Rev. Lett. **57**, 2897 (1986);
M. Gruwe *et al.* (CHARM-II), Phys. Lett. B **309**, 463 (1993);
K.S. McFarland *et al.* (CCFR), Phys. Rev. Lett. **75**, 3993 (1995);
F. Dydak *et al.* (CDHS), Phys. Lett. B **134**, 281 (1984); CHORUS Proposal, *CERN-SPSLC/90-42* (1990).

[4] C. Athanassopoulos *et al.* (LSND), Phys. Rev. Lett. **77**, 3082 (1996); Phys. Lett. C **54**, 2685 (1996).

[5] NOMAD Collaboration, J. Altegoer *et al.*, Nucl. Instrum. Methods A **404**, 96 (1998).

[6] G. Acquitaspace *et al.*, *CERN-ECP/95-14* (1995).

[7] GEANT 3.21, *CERN Progr. Libr. W5013* (1994).

[8] A. Ferrari and P. R. Sala, *Proc. MC93 Int. Conf.*, Tallahasee, Florida (1993).

[9] G. Ambrosini *et al.*, *SPY Proposal, CERN-SPSLC/96-01, SPSLC/P294* (1996).

[10] L. Borodovsky *et al.* (BNL 776), Phys. Rev. Lett. **68**, 274 (1992);
B. Bodmann *et al.* (KARMEN), Nucl. Phys. A **553**, 831c (1993);
K. S. McFarland *et al.* (CCFR), Phys. Rev. Lett. **75**, 3993 (1995).

[11] R. D. Cousins and V. L. Highland, Nucl. Instrum. Methods A **320**, 331 (1992).

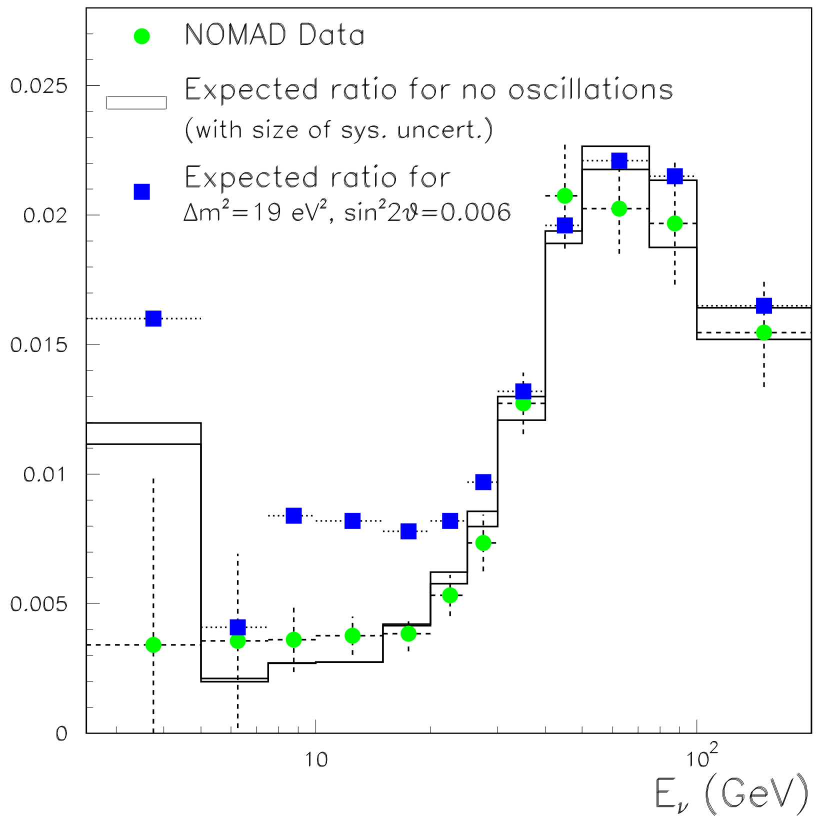

Figure 12: Observed $\mathcal{R}_{e\mu}$, compared to expectations in absence of oscillations and to oscillations with $\sin^2 2\theta = 0.006, \Delta m^2 = 19\ e\mathrm{V}^2$.

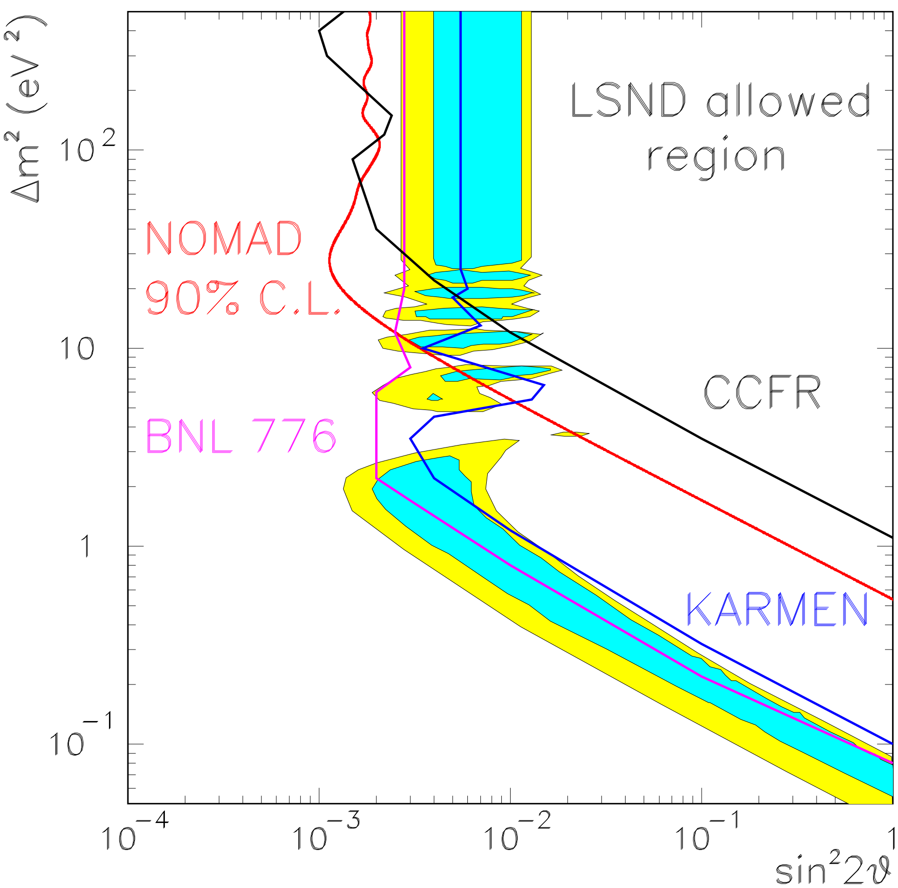

Figure 13: Preliminary exclusion plot on the oscillations parameters plane, obtained using 1995 NOMAD data. The limits[10] of other experiments and the LSND-allowed region are shown as well.

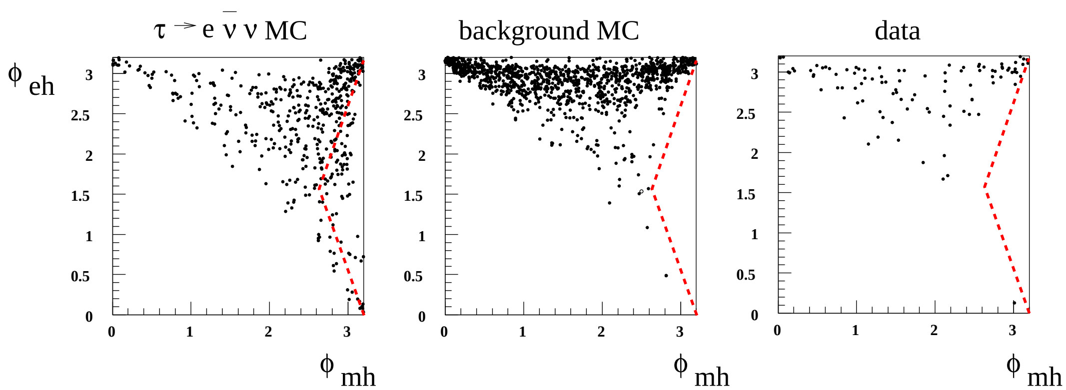

Figure 14: Distributions of ϕ_{eh} vs ϕ_{mh} obtained after $\tau^- \rightarrow e^-\nu_\tau\bar{\nu}_e$ selection cuts have been applied.

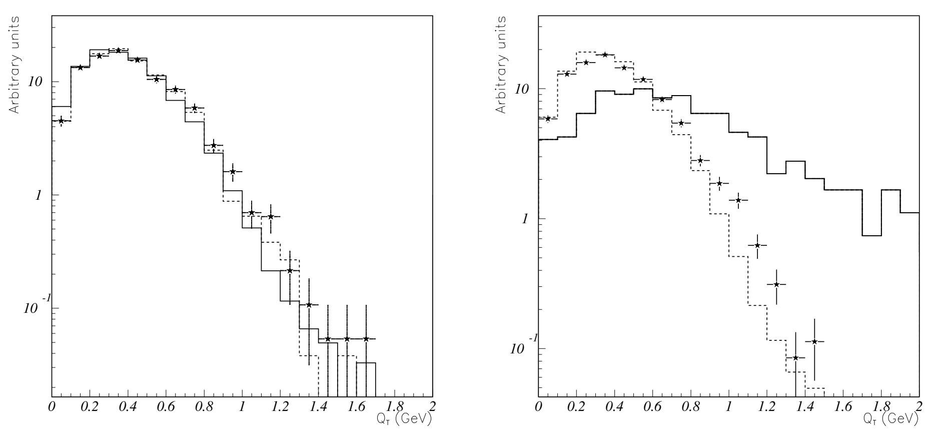

Figure 15: Left: Q_T distributions for NC MC sample (solid line), CC MC events with μ^- removed (dashed line), and "data simulator" (real ν_μ CC events with μ^- removed). Right: Q_T distributions for simulated $\tau^- \rightarrow \pi^-\nu_\tau$ decays (solid line), neutral current background from MC (dashed line), and real data after all the cuts except Q_T have been applied.